Journal of Materials Chemistry

Dynamic Article Links

Cite this: J. Mater. Chem., 2012, 22, 19039

www.rsc.org/materials

PAPER

# Role of crystal defects in red long-lasting phosphorescence of $CaMgSi_2O_6$:Mn diopsides†

**Aurélie Bessière,*[ab] Aurélie Lecointre,[a] K. R. Priolkar[b] and Didier Gourier[a]**

*Received 10th May 2012, Accepted 21st July 2012*
**DOI: 10.1039/c2jm32953k**

$CaMgSi_2O_6$:Mn diopsides are used for *in vivo* long-lasting phosphorescence (LLP) imaging. Trapping defects involved in the LLP mechanism were investigated. On annealing Mn-doped diopsides at 1100 °C in an Ar–$H_2$ atmosphere, Ca EXAFS/XANES and electron paramagnetic resonance (EPR) evidenced paramagnetic oxygen vacancies while X-ray diffraction, Mn XANES and EPR revealed $SiO_2$ formation and significant evaporation of the Mn dopant. A thermally stimulated luminescence (TSL) peak at 475 K ascribed to electron trapping at oxygen vacancies was found responsible for LLP at RT. Most intense red LLP suitable for *in vivo* imaging was achieved by a trade-off between a high $Mn^{II}$ content (favourable to $Mn^{II}_{Mg}$ red over $Mn^{II}_{Ca}$ orange luminescence) and the formation of oxygen vacancies favourable to LLP and luminescence light yield. Mn XANES revealed an effective charge larger than 2+ for $Mn^{II}$, in line with the role of hole trap in the LLP mechanism. Compounds annealed at lower temperatures (800 °C and 900 °C) in Ar–$H_2$ showed smaller particle size (60–70 nm) and maximum Mn content but poor luminescence and LLP due to surface quenching defects.

## 1. Introduction

Persistent luminescence also called long-lasting phosphorescence (LLP) or long afterglow has been known for several centuries since the first material, for which this property was observed, the famous Bolognian stone, was discovered in 1602 by the Italian Vincenzo Casciarolo.[1] The Bolognian stone could emit blue-violet light for a couple of minutes in the dark due to its barium sulfur content. This phenomenon was further investigated in the 17$^{th}$ century and more materials were gradually discovered over the following centuries. However this is only in the most recent period, from the mid-1990s, that LLP gained a renewed interest with the discovery of the famous bright persistent phosphor $SrAl_2O_4:Eu^{2+}$, $Dy^{3+}$ by Matsuzawa *et al.*[2] Since then, more and more persistent phosphors have been reported every year and the growing community now focuses on the underlying mechanisms. Explaining the LLP mechanism has ever been a challenging goal as a wide diversity of charge trapping and detrapping processes are possible at any defect in the arrangement of the atoms of a crystalline material. One possible way to create/enhance LLP is to add, as a co-dopant, a trivalent lanthanide ion ($Ln^{3+}$) in addition to the main luminescent doping ion. Even though this is a popular strategy, there is often a controversy about the role of these co-dopants. One can cite various examples. On the one hand $YPO_4$:(Ce/Pr/Tb)$^{3+}$, $Ln^{3+}$ are model compounds and have been designed in a way that $Ln^{3+}$ clearly behaves as the electron trap responsible for the delayed release of electrons and the subsequent recombination of the latter on the hole trap and luminescent centre constituted by either $Ce^{3+}$ (ref. 3), $Pr^{3+}$ (ref. 4) or $Tb^{3+}$.[5] On the other hand the mechanism is still unclear in the well-known $Eu^{2+}$-doped strontium aluminate. While $Eu^{2+}$ LLP was greatly improved by $Dy^{3+}$ co-doping,[2] some authors remarked that it still existed without co-doping[6] and therefore some intrinsic traps should be responsible for the LLP phenomenon. This famous example is actually representative of many $Ln^{3+}$ co-doped materials whose intrinsic structure is able to produce LLP without co-doping. Therefore it appears that intrinsic defects in LLP phosphors should be deeply investigated as they may play a major role.

$Mn^{II}$-doped diopsides $CaMgSi_2O_6:Mn^{II}$ are red LLP phosphors used to develop a novel application for small animal *in vivo* imaging.[7,8] Similarly to the example of strontium aluminate, they show enhanced red persistent luminescence with $Dy^{3+}$ (ref. 9) or $Pr^{3+}$ co-doping.[7] Moreover blue and white persistent luminescence has been reported in two diopsides, $CaMgSi_2O_6:Eu^{2+}$, $Ln^{3+}$ (Ln = Dy, Nd)[10] and $CaMgSi_2O_6:Dy^{3+}$ (ref. 11), respectively. The $Mn^{II}$-singly-doped diopside also shows some LLP, especially with a high doping content of $Mn^{2+}$ ions.[12] In order to elucidate the LLP mechanism in $Mn^{II}$-doped and later on in ($Mn^{II}$, $Ln^{3+}$)-co-doped diopsides, we present here a study of several manganese-doped diopsides prepared by a sol–gel method. We will show that the most crucial synthesis parameters to create intrinsic

[a]*Chimie Paristech, Laboratoire de Chimie Matière Condensée de Paris, UPMC, Collège de France, UMR - CNRS 7574, 11 rue Pierre et Marie Curie, 75231 Paris Cedex 05, France. E-mail: aurelie-bessiere@chimie-paristech.fr*
[b]*Department of Physics, Goa University, Taleigao Plateau, Goa 403 206, India*

† Electronic supplementary information (ESI) available. See DOI: 10.1039/c2jm32953k

defects in the structure are the atmosphere and temperature of the last annealing step of the sol–gel synthesis. X-ray absorption spectroscopy (XAS) and electron paramagnetic resonance (EPR) techniques were used to investigate manganese-doped diopsides prepared by varying these parameters and identify the charge-trapping defects responsible for LLP in these materials.

## 2. Experimental

The diopside compounds were prepared by a sol–gel method. Stoichiometric quantities of $Ca(NO_3)_2 \cdot 4H_2O$ (99.98% metal basis), $Mg(NO_3)_2 \cdot 6H_2O$ (99% A.C.S. reagent) and the required doping quantity of $MnCl_2 \cdot 4H_2O$ (purum p.a >99%) were dissolved in water previously acidified with nitric acid to pH = 2. The nominal molar ratios of the Mn dopant were 2.5% relative to the number of (Ca + Mg) cations. A stoichiometric amount of tetraethoxysilane was added to the solutions which were then vigorously stirred at room temperature (RT) for one hour until homogeneous liquid sols were obtained. Gelification of the sols was accelerated by placing the latter in a closed vessel at 70 °C for one hour. The obtained transparent gels were dried overnight at 110 °C. A last annealing step was carried out by firing the solid gels at various temperatures under various atmospheres. Five compounds with different annealing treatments were prepared. They are reported along with short names in Table 1. The white pieces of compounds were finely ground in an agate mortar before characterization.

X-Ray Diffraction (XRD) was performed on a Panalytical X'Pert Pro diffractometer with an incident-beam Ge (111) monochromator, at $U = 45$ kV and $I = 40$ mA.

X-ray absorption fine structure (EXAFS) was measured at the Ca K and Mn K-edge in transmission and fluorescence modes, respectively, at the EXAFS-1 Beamline at the Elettra Synchrotron Source using Si (111) as the monochromator. The absorbers for transmission were prepared by sprinkling fine powder of the sample on a Scotch tape and stacking such layers until total absorption beyond the edge was about 2.5. For fluorescence measurements absorbers were prepared by depositing the powder sample on a membrane. The incident X-ray flux was monitored by a gas filled ionization chamber. The monochromator was detuned by 40% to avoid higher harmonics. Fluorescence yield was detected using a silicon drift detector. An aluminum filter was used to take care of calcium fluorescence lines. Data analysis was carried out using IFEFFIT in ATHENA and ARTEMIS programs.[13,14] Here theoretical fitting standards were computed with FEFF6.[15,16] The data in the $k$ range of (2–12) $Å^{-1}$ were used for analysis. Full multiple scattering calculations of the Mn K edge XANES were performed using FEFF8.4.[17] Mn was placed at the Mg site of $CaMgSi_2O_6$ structure[18] in ATOMS 3.0 (ref. 15) to generate the atomic coordinates. For the FEFF calculations spherical muffin tin potentials were self consistently calculated over a radius of 8 Å. Default overlapping muffin tin potentials and Hedin–Lunqvist exchange correlations were used to calculate X-ray absorption transitions to a fully relaxed final state in the presence of a core hole. An energy shift of 2 eV was applied to achieve a better description of pre-edge absorption at the Mn K edge.

X-band electron paramagnetic resonance (EPR) measurements were performed at room temperature with a Bruker Elexsys E500 spectrometer with a Super-High-Q cavity using a microwave frequency of 9.4 GHz (X-band), microwave power of 2 mW and modulation field of 10 Gauss. $Mn^{II}$ spectra were recorded in the usual in-phase detection mode, while oxygen vacancies were detected in the 90° out-of-phase (phase quadrature) detection mode according to their long relaxation times.

X-ray excited optical luminescence (XREOL), LLP and thermally stimulated luminescence (TSL) measurements were conducted on 13 mm diameter and 1 mm thick pellets made of the powder samples. X-ray irradiation was provided by a molybdenum tube operated at $V = 50$ kV and $I = 20$ mA. In XREOL and LLP, X-ray irradiation was performed at 45° angle of the pellet while luminescence was being detected at 45° angle by an optical fibre connected to a CCD camera coupled to a monochromator. The shutter aperture time of the CCD camera was set to 1 second. In TSL the pellet was fixed with silver glue on the cold finger of a closed cycle helium cryostat. X-ray irradiation was performed through a thin beryllium window of the cryostat at 45° angle. Luminescence was detected through a quartz window of the cryostat at 45° angle, by an optical fibre connected to a CCD camera coupled with a monochromator. In TSL the sample was first irradiated for 10 min at 30 K. Luminescence was then detected while a heating rate of 10 K $min^{-1}$ was being applied up to 650 K. The shutter aperture time of the CCD camera was set to 1 second.

**Table 1** $CaMgSi_2O_6$:Mn compounds with 2.5 at.% nominal Mn content prepared under various annealing conditions. "Ar–$H_2$" indicates a thermal treatment carried out under a 90% argon + 10% hydrogen flux (Noxal 4). "Ar–$H_2$+" indicates that the gas flow was twice more important than the flow of "Ar–$H_2$". In a compound name such as "D800H", D stands for diopside, 800 is the annealing temperature in °C and H is the hydrogenated atmosphere. A stands for air

| Thermal treatment | 800 °C Ar–$H_2$ | 900 °C Ar–$H_2$ | 1100 °C Ar–$H_2$ | 1100 °C Ar–$H_2$+ | 1100 °C air |
|---|---|---|---|---|---|
| Sample name | D800H | D900H | D1100H | D1100H+ | D1100A |

## 3. Results and discussion

### 3.1 Characterization of structural defects

The XRD patterns of Mn-doped diopsides prepared under different annealing conditions are presented in Fig. 1. They all showed Bragg peaks belonging to diopsides (JCPDS 17-0318). The patterns for the lowest annealing temperatures (800 °C and 900 °C) displayed broadened peaks due to nanoparticles formation. Transmission electron microscopy images (not shown) confirmed the synthesis of tens of nanometers large particles allowing their dispersion in a physiological medium and their subsequent injection to small animals for *in vivo* imaging.[7] By increasing the annealing temperature, Bragg peaks narrowed down, evidencing longer crystal order and larger particles size. The following Scherrer formula was used to evaluate the particles size:

$$D = k\lambda/\beta\cos\theta$$

where $D$ is the crystal order length, $k$ the Scherrer constant ($k = 0.9$), $\lambda$ the $K_\alpha$ Cu radiation wavelength, $\beta$ the full width at

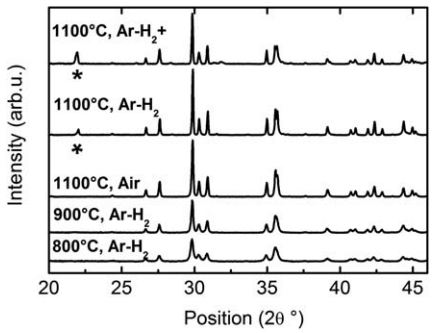


**Fig. 1** XRD patterns of $CaMgSi_2O_6$:Mn compounds annealed under various conditions. * indicates $SiO_2$ impurity.

half maximum and $\theta$ the diffraction angle. By increasing the annealing temperature from 800 °C to 900 °C and further on to 1100 °C the particles size varied from 59 (± 10) nm to 69 (± 10) nm and to >200 nm, respectively.

In the diffraction patterns of the compounds annealed at 1100 °C in an Ar–$H_2$ atmosphere (D1100H and D1100H+) an impurity peak could also be distinguished at $2\theta = 22.0°$ and attributed to cristobalite $SiO_2$. This impurity peak was found to be twice more intense in D1100H+ annealed under strong reducing conditions than in D1100H annealed under mild reducing conditions. The compound annealed at the same temperature in air D1100A did not show any impurity peak. Therefore a high annealing temperature together with a reducing atmosphere led to $SiO_2$ crystallisation and therefore most probably to the partial decomposition of the diopside structure. The evaporation of complementary elements was therefore also likely, *i.e.* for instance stoichiometric amounts of, on the one hand, calcium, manganese and/or magnesium and on the other hand oxygen atoms. This point will be further discussed in the following.

EPR spectra of the five investigated diopsides are presented in Fig. 2. The inset (a) shows a close-up of D1100H+ spectrum where a typical but very weak signal from $Mn^{II}$ ions ($S = 5/2$, $I = 5/2$) in octahedral field was identified. The spectrum displayed a central set of 6 hyperfine lines corresponding to the $|1/2> \leftrightarrow |-1/2>$ fine

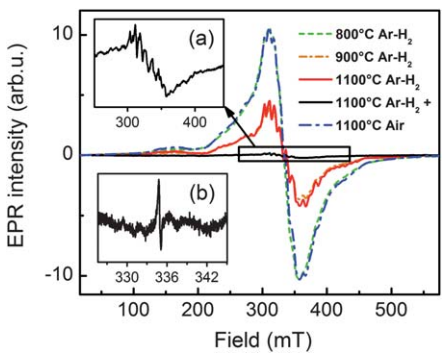


**Fig. 2** X-band EPR spectra at room temperature of $CaMgSi_2O_6$:Mn compounds annealed under various conditions. Insets: (a) zoom of the EPR spectrum of the compound annealed at 1100 °C in Ar–$H_2$ + (D1100H+). (b) EPR spectrum recorded in the 90° out-of-phase detection mode (microwave power: 0.2 mW, modulation amplitude: 10 Gauss) of the compound annealed at 1100 °C in Ar–$H_2$ (D1100H), revealing paramagnetic oxygen vacancies.

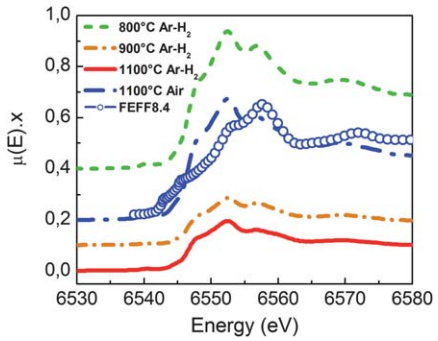


**Fig. 3** Unnormalized Mn K edge absorption spectra of $CaMgSi_2O_6$:Mn compounds annealed under various conditions. Mixed line: calculated XANES spectrum of D1100A using FEFF8.4 software.

structure transition at $g_{eff} = 2$ as well as four weaker signals in the flank of the central transition corresponding to $|\pm1/2> \leftrightarrow |\pm3/2>$ and $|\pm3/2> \leftrightarrow |\pm5/2>$ transitions. It was shown in ref. 12 that most of the doping manganese ions substitute magnesium sites where they adopt an elongated octahedral environment. It was striking to observe in Fig. 2 that although Mn nominal concentration was identical for all the compounds (2.5%), large differences in $Mn^{II}$ EPR signal intensities were observed. Since a variation of annealing atmosphere and temperature was involved, either a change in Mn valence state or a Mn loss from the solid was responsible for the changes in EPR intensities.

Unnormalized Mn K edge absorption spectra presented in Fig. 3 were recorded to test these two hypotheses. Shape and position of spectra were all similar evidencing no significant change in the manganese valence state. As the absorber thickness was kept constant for all the samples, the absorption jump could be directly related to the number of manganese absorbing ions. Absorption jump values under the absorption curves were therefore presented, relative to the one of D800H, in Fig. 4, together with $Mn^{II}$ EPR intensities relative to the EPR intensity of D800H. For all the five diopside compounds, the absorption jump intensities showed a very similar evolution to the EPR intensities. The most intense Mn signal was found for annealing treatments performed either at low temperature (800 °C) in Ar–$H_2$ or in air at 1100 °C. The increase of the annealing temperature to 900 °C and further on to 1100 °C in Ar–$H_2$ induced a manganese loss of about 60% according to both EPR and XANES. Reducing annealing efficiently drove the evaporation

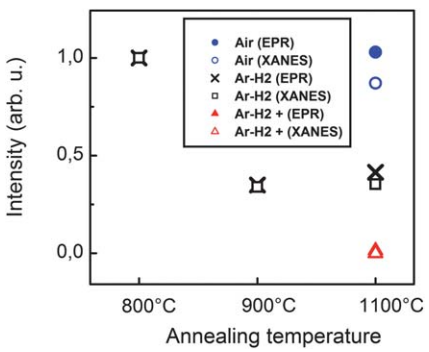


**Fig. 4** Intensities of EPR signal (full symbols) and Mn K edge absorption jumps (open symbols) relative to compound D800H.

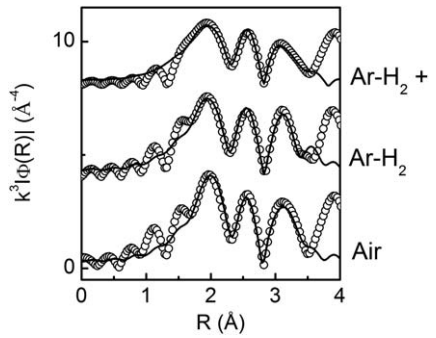


**Fig. 5** Magnitude of Fourier transforms of $k^3$ weighted EXAFS of Ca K-edge of $CaMgSi_2O_6$:Mn compounds annealed at 1100 °C under various atmospheres.

of manganese ions out of the diopside structure. This was further confirmed by the huge loss of manganese ions observed when annealing was performed under stringent reducing conditions at 1100 °C on D1100H+. The EPR signal was found to drop by 98% in D1100H+ relative to D800H and even though it was attempted, no manganese absorption edge could be detected in D1100H+.

The departure of manganese ions from $CaMgSi_2O_6$ structure raised the question of whether it was accompanied by the formation of oxygen vacancies or not. Extensive EXAFS studies at Ca K edge were conducted to investigate a possible oxygen loss. Ca K edge EXAFS spectra of diopsides prepared in air, Ar–$H_2$ and Ar–$H_2$+ at 1100 °C are shown in Fig. 5. Data fitting shown in Fig. 5 resulted in Ca–O bond lengths and coordination numbers presented in Table S1 of the ESI.† Ca–O bond lengths were not found to vary much with annealing conditions whereas Ca–O coordination numbers for the nearest O atoms were found to clearly decrease along with the atmosphere reducing character. Fig. 6 displays the Ca–O coordination numbers extracted from EXAFS analysis distinguishing various types of oxygen atoms. As shown in Fig. 6, O3 is shared by two adjacent $SiO_4$ tetrahedra ("bridging" oxygen) while O1 and O2 are less tightly bound. The nearest Ca–O distances concerned O1 and O2 oxygen and were found to decrease with reducing annealing character whereas the second nearest distance relative to the Ca–O3 bond was found to be constant. The results therefore show that O1 and O2 oxygen vacancies were formed around calcium when the compounds were prepared in a reducing atmosphere and that the oxygen vacancies number increased with Ar–$H_2$ flow.

Additional evidences of oxygen vacancies were provided by the normalised Ca K-edge XANES spectra of the compounds (Fig. 7). Pre-edge features showed an intensity increase with Ca site symmetry reduction, as can be more clearly seen in the inset of Fig. 7. This site symmetry reduction is the result of the reduction in number of oxygen neighbours around calcium with increased Ar–$H_2$ flow. Secondly a change was also noticed in the main peak of X-ray absorption spectra. A decrease of the main peak intensity was observed with increasingly stringent reducing conditions. As the absorption process is a transition to unoccupied states, a decrease in intensity of the absorption peak or the area under the peak implies a decrease in unoccupied density of states. In these compounds, the unoccupied density of states around Ca is composed of calcium as well as oxygen states. A decrease in area under the absorption curve may therefore mean a decrease in available oxygen states which corroborates EXAFS data showing less oxygen atoms around calcium with Ar–$H_2$ flow increase.

EXAFS at Mn-K-edge spectra with best fits are shown in the ESI (Fig. S2†). Table S1† displays the fitting parameters. No significant change was found in distances or coordination numbers between compounds. In contrast to calcium no oxygen vacancy was therefore evidenced in the first coordination sphere of Mn dopants.

EPR spectroscopy was conducted to characterize further oxygen vacancies. The corresponding signal should occur in the $g = 2.002$ region, which is dominated by the intense and broad spectrum of $Mn^{II}$. However the relaxation times T1 and T2 of oxygen vacancies are very long in $SiO_2$ and in silicates, so that their EPR spectra can be selectively detected in 90° out-of-phase (phase quadrature) detection mode with respect to the modulation field.[19] The phase quadrature spectrum is presented in the inset (b) of Fig. 2 for the compound D1100H. It showed a unique signal at $g = 1.999$, characteristic of an E′ center formed by an oxygen vacancy with one unpaired electron ($S = 1/2$). Contrary to alkali halides and ionic oxides where the unpaired electron lies in the vacancy, the unpaired electron in $SiO_2$ and silicates lies in a non-bonding silicium $sp^3$ orbital, giving a typical EPR signature.[20]

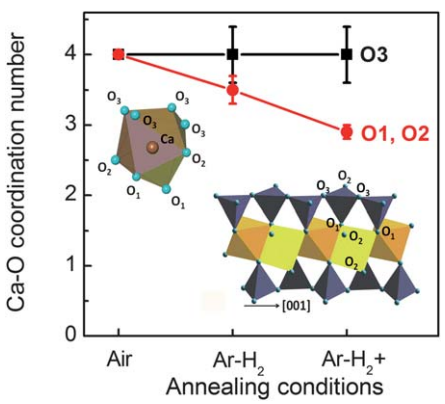


**Fig. 6** Ca–O coordination numbers as obtained by fitting EXAFS Ca K edge spectra of $CaMgSi_2O_6$:Mn compounds annealed under various conditions.

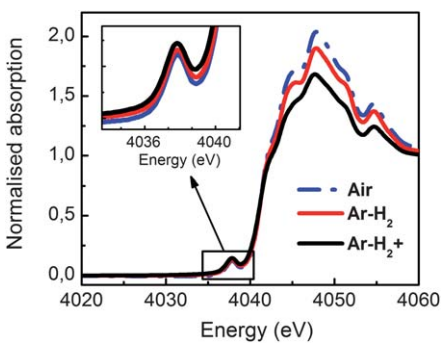


**Fig. 7** Ca K edge absorption spectra of $CaMgSi_2O_6$:Mn compounds annealed at 1100 °C in various atmospheres. Inset: zoom of the pre-edge domain.

Finally the calculated XANES spectrum of D1100A using FEFF8.4 is shown as a mixed line in Fig. 3. Although the main absorption features were reproduced by the calculation some significant discrepancies appeared. The major one was the position of the absorption edge itself. According to FEFF calculations, in the diopside structure with $Mn^{II}$ occupying octahedral Mg positions, Mn K edge (first maximum in the derivative spectra) occurred at 6541 eV whereas the experimental spectrum indicated the edge to be at 6543 eV, which is 2 eV higher than that in the calculated spectrum. This higher edge energy indicates that the effective charge on Mn in the diopside is actually higher than 2+. This appears in line with the tendency of the $Mn^{II}$ dopant to trap holes in $CaMgSi_2O_6$ as it was hypothesized in ref. 12. Furthermore, the intensity of the pre-peak was also stronger in the experimental curve than in the calculated one. In octahedral symmetry, the p–d hybridization of the metal ligand states is forbidden and hence the pre-peak is usually due to quadrupole transition. The intensity of such quadrupolar transitions is usually very weak as can be seen in calculated spectra. Consequently the stronger pre-peak in the experimental curve pointed to the presence of distorted octahedral environment around Mn. Analysis of Mn K EXAFS has shown that, of the six oxygen atoms surrounding Mn, two are much distant than the other four. These distortions are responsible for a higher effective charge on Mn.

### 3.2 Role of defects in X-ray excited optical luminescence

X-ray excited optical luminescence (XREOL) spectra of all the compounds are presented in Fig. 8. The XREOL behaviour of $CaMgSi_2O_6$:$Mn^{II}$ has already been investigated in detail in ref. 12. The spectra displayed two broad emission bands at 585 nm and 685 nm ascribed to the $^4T_1$ ($^4G$) → $^6A_1$ ($^6S$) d–d transition of $Mn^{2+}$ substituting $Ca^{2+}$ (denoted as $Mn^{II}_{Ca}$) and $Mn^{II}$ substituting $Mg^{2+}$ (denoted as $Mn^{II}_{Mg}$), respectively. It was also shown that for Mn nominal doping ≥2.5% with a preparation at 1100 °C in Ar–$H_2$, $Mn^{II}$ substituted almost exclusively $Mg^{2+}$ sites in the diopside structure.[12] However a small residual amount of $Mn^{II}$ was always present at the calcium site irrespective of the nominal Mn content, giving rise to an intense emission at 585 nm. The reason for such a high intensity is the non-centrosymmetry of the calcium site compared to the centrosymmetry of the magnesium site, which makes the spin and symmetry forbidden $^4T_1(^4G)$ → $^6A_1(^6S)$ emission far more efficient for $Mn^{II}_{Ca}$ than for $Mn^{II}_{Mg}$.

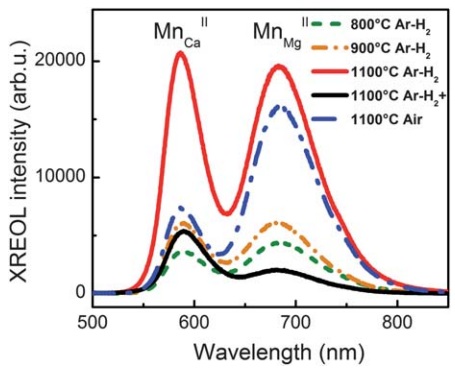


**Fig. 8** X-ray excited optical luminescence (XREOL) spectra of $CaMgSi_2O_6$:Mn compounds annealed under various conditions.

The noticeable differences in XREOL spectra between the five diopsides shown in Fig. 8 were explained on the basis of the present structural study. The compound annealed at 800 °C showed a weak XREOL intensity although its strong $Mn^{II}$ EPR signal shown in Fig. 4 evidenced that D800H possessed the highest $Mn^{II}$ content of all compounds. Moving from the diopside annealed at 800 °C to the one annealed at 900 °C, XREOL intensity was enhanced by about 25% (see Fig. 8). Yet the $Mn^{II}$ content in D900H was less than half its content in D800H according to both EPR and XANES spectra (*cf.* Fig. 4). When increasing the annealing temperature from 800 °C to 900 °C, no significant amount of oxygen vacancies was detected according to EXAFS, but the particles size and/or crystal order were shown to increase. The XREOL light yield enhancement may therefore have two origins: (i) a lower Mn content in D900H than in D800H suppressed a possible quenching phenomenon by dopant concentration; (ii) otherwise and most probably, as the particles size and crystal order increased when moving from D800H to D900H, luminescence quenching by defects, mainly at the particles surface, was reduced. In the following more evidence will be given in favour of this second hypothesis.

Fig. 8 shows that moving from an annealing temperature of 900 °C to 1100 °C in Ar–$H_2$ led to a 200% XREOL intensity increase though both D900H and D1100H presented a similar $Mn^{II}$ content according to EPR and XANES (*cf.* Fig. 4). Hence the luminescence enhancement with increasing annealing temperature did not originate from a reduced quenching phenomenon by dopant concentration. It was therefore clearly induced by a reduction of the number of (surface) defects acting as quenching centres, a consequence of the particles size increase with increasing annealing temperature.

In Fig. 8 the diopside annealed in intense Ar–$H_2$ flow (D1100H+) presented a strongly diminished XREOL intensity relative to D1100H. This was directly related to the $Mn^{II}$ content in the samples as the latter was shown to drop by more than 95% when moving from D1100H to D1100H+ according to both EPR and XANES. Furthermore the large number of oxygen vacancies present in D1100H+ may imply a very disordered lattice with non-radiative recombination centres that hinder luminescence, explaining why not only $Mn^{II}_{Mg}$ but also $Mn^{II}_{Ca}$ emission was diminished (as $Mn^{II}_{Ca}$ concentration may be similar in all samples as shown in ref. 12).

Finally Fig. 4 shows that the diopside annealed in air at 1100 °C contained the same amount of $Mn^{II}$ as the diopside annealed in Ar–$H_2$ at 900 °C. In Fig. 8 its XREOL intensity was enhanced relative to the latter. Therefore as the improvement was not due to different dopant content, it was again ascribed to particles size increase and better crystal order when moving from D900H to D1100A. Both D1100H and D1100A compounds were annealed at the same temperature and therefore presented similar particle sizes. Furthermore D1100A was shown to contain more than twice more $Mn^{II}$ ions than D1100H. Nevertheless D1100A presented a 15% decrease in the $Mn^{II}_{Mg}$ XREOL intensity and a 60% decrease in the $Mn^{II}_{Ca}$ XREOL intensity compared to D1100H. The mild reducing annealing treatment at 1100 °C was therefore highly beneficial to $Mn^{II}$ ions luminescence efficiency. The EXAFS and EPR studies presented for both D1100A and D1100H here above revealed oxygen vacancies in the compound annealed in Ar–$H_2$ flow. These vacancies, which are not in the

first neighbouring position with respect to $Mn^{II}$ ions, may have disturbed the symmetry around $Mn^{II}$ allowing the mixing of opposite parity orbitals and hence making $^4T_1 \rightarrow {}^6A_1$ transitions more efficient.

### 3.3 TSL and charge trapping

TSL measurements were conducted to characterize charge trapping phenomena and long-lasting phosphorescence. The compounds were excited by X-rays for ten minutes at 30 K while carriers were being trapped. Then by applying a temperature ramp and simultaneously detecting TSL, an "energetic map" of charge-trapping defects can be drawn as electrons/holes are detrapped for each defect at a specific temperature. A TSL peak corresponds to an amount of thermal energy needed to detrap the charge (electron or hole) and promote its radiative recombination with its counter-charge (hole or electron) at/near a luminescent center. Below room temperature, TSL peaks are relative to shallow traps (typically below 0.8 eV) while above room temperature peaks relate to deeper traps (from 0.8 eV to 2 eV). TSL intensity observed between 300 K and 500 K typically refers to long-lasting phosphorescence behaviour at RT.

TSL glow curves are plotted in Fig. 9(a) and (b) for $Mn^{II}_{Mg}$ emission at 685 nm and $Mn^{II}_{Ca}$ emission at 585 nm, respectively. By comparing photoluminescence, X-ray excited optical luminescence and long-lasting phosphorescence spectra, we had concluded in ref. 12 that $Mn^{II}_{Mg}$ was the preferential hole trapping centre relative to $Mn^{II}_{Ca}$ during X-ray irradiation. This preferential trapping was even enhanced as the total content of $Mn^{II}$ ions was high in the compound. Again for most of the compounds here the TSL intensity of $Mn^{II}_{Ca}$ (Fig. 9(b)) was lower than the one of $Mn^{II}_{Mg}$ (Fig. 9(a)). Nevertheless this was less pronounced for D1100H and D900H, which had an intermediate $Mn^{II}$ content, and not true anymore for D1100H+ which contained only very few $Mn^{II}$ and therefore showed more intense TSL through $Mn^{II}_{Ca}$ than through $Mn^{II}_{Mg}$. Hence the compounds with the highest $Mn^{II}$ content according to Fig. 4 (D800H and D1100H) had the lowest $Mn^{II}_{Ca}$ TSL intensity. The amount of $Mn^{II}_{Ca}$ TSL intensity therefore appeared directly related to the quantity of $Mn^{II}$ present in the compounds: as more $Mn^{II}$ entered the structure, more $Mn^{II}$ ions substituted the magnesium site, and acted as preferential hole traps. Hence less luminescence was emitted from $Mn^{II}_{Ca}$. This may also be true for X-ray excited optical luminescence as the mechanism also partially proceeds from hole trapping and is *a fortiori* true for TSL where the hole trapping step is compulsory.

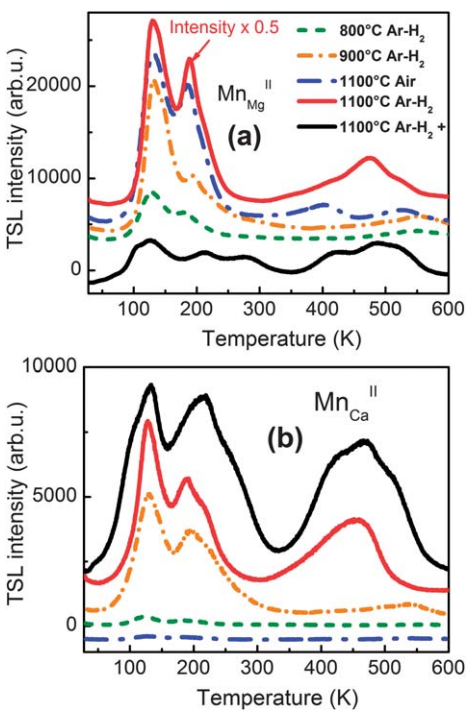


**Fig. 9** Thermally stimulated luminescence (TSL) glow curves of $CaMgSi_2O_6$:Mn compounds annealed under various conditions (a) emission of $Mn^{II}_{Mg}$ at 685 nm and (b) emission of $Mn^{II}_{Ca}$ at 585 nm.

TSL glow curves of D800H and D900H shown in Fig. 9(a) were very similar in shape. They presented mainly high intensity peaks below room temperature and a broad low-intensity band around 550 K. Below RT the luminescence intensity of D900H was about twice as intense as the one of D800H. This was similar to the comparison of XREOL intensities and again this was certainly due to less quenching by surface defects in D900H. Similarly to the evolution in XREOL, the TSL intensity of D1100H below RT was greatly enhanced compared to D900H (Fig. 9(a)). When moving to D1100A, the TSL intensity below RT was enhanced relative to D900H because of an increased particle size but was reduced compared to D1100H because of less oxygen vacancies that were beneficial for XREOL light yield.

At temperature ≥RT, new TSL peaks arose when the annealing temperature reached 1100 °C. A broad band peaking at 400 K was observed irrespective of the atmosphere, while a very intense peak at 475 K appeared with a reducing atmosphere. Under strongly reducing conditions (D1100H+) the overall intensity was strongly reduced relative to D1100H. This may be primarily due to a very low $Mn^{II}$ content as evidenced by EPR and XANES. The origin of the peak at 400 K is still unclear as our measurements in EPR and X-ray absorption spectroscopies did not evidence any identified defect for an annealing at 1100 °C in air. As it appears at 1100 °C in a reducing atmosphere and not in air, the 475 K peak was ascribed to oxygen vacancies that were evidenced in EXAFS and XANES analyses.

Decays of LLP intensities at peaks maxima, *i.e.* at 585 nm (scattered points) and at 685 nm (lines), are shown in Fig. 10(a) for the four main samples (900 °C is not shown for clarity purpose). LLP intensity appears clearly correlated with TSL intensity between 300 K and 500 K. The most intense 685 nm LLP decays are observed for D1100H and D1100H+ which present the most intense 685 nm TSL intensity in the 300–500 K range. The LLP intensity at 585 nm is almost zero for D800H and D1100A just as their 585 nm TSL intensity between 300 K and 500 K. D1100A does not show any TSL peak at 475 K (oxygen vacancies) and therefore presents an order of magnitude lower LLP intensity than D1100H after 20 minutes.

The scheme of Fig. 10(b) summarizes the effects of the three main TSL peaks above RT. As holes are mainly trapped at $Mn^{II}_{Mg}$ sites, TSL peaks represent detrapping of electrons from defects, followed by electron–hole recombination and emission of $Mn^{II}_{Mg}$. The 475 K TSL peak ascribed to oxygen vacancies has the most important effect on LLP at 20 minutes (dotted line in Fig. 10(b)).

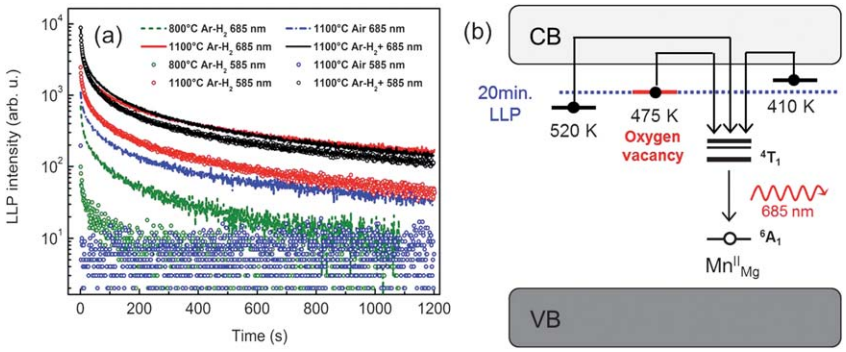


**Fig. 10** (a) Long-lasting phosphorescence (LLP) decay curves of $CaMgSi_2O_6$:Mn compounds annealed under various conditions after 10 min. X-ray irradiation (b) mechanism scheme showing electron detrapping and recombination with hole left on $Mn^{II}_{Mg}$.

Therefore an annealing step at 1100 °C in Ar–$H_2$ is essential to produce oxygen vacancies and induce the most intense LLP in the material.

## 4. Conclusions

The paper is amongst the first studies involving X-ray absorption spectroscopy applied to LLP materials. Very distinct features within the five manganese-doped diopsides were extracted from Ca K-edge and Mn K-edge EXAFS and XANES investigation. Several converging results from Ca EXAFS/XANES and Mn EXAFS evidenced the formation of oxygen vacancies that are not in the first neighbouring position with respect to manganese ions on annealing at 1100 °C in an Ar–$H_2$ atmosphere. EPR confirmed the presence of paramagnetic oxygen vacancies in the material annealed in Ar–$H_2$ at 1100 °C. Furthermore, on annealing in Ar–$H_2$, Mn XANES and $Mn^{II}$ EPR agreed on a significant evaporation of the manganese dopant out of the $CaMgSi_2O_6$ structure accompanied by $SiO_2$ formation assessed by XRD. The investigation of Mn K-edge XANES of manganese-doped $CaMgSi_2O_6$ also revealed a tendency for $Mn^{II}_{Mg}$ to adopt a higher effective charge in comparison to $Mn^{2+}$ and therefore to actually constitute a hole trap in $CaMgSi_2O_6$. Taken together, all these structural data converge to interpret the luminescence properties of $CaMgSi_2O_6$:Mn prepared by a sol–gel method.

Annealing treatments at 800 °C and 900 °C in Ar–$H_2$ enabled the preparation of pure diopside nanoparticles with small particle size (60–70 nm) and with a maximum content of manganese dopant, probably close to the nominal introduction (2.5 at%). However these annealing temperatures were too low to promote intense luminescence. This was ascribed to numerous quenching defects arising from poor crystal order and high particles surface/volume ratio. Besides no long-lasting phosphorescence was to be expected as no defects associated with TSL peaks between 300 and 500 K were present.

Annealing at 1100 °C was highly beneficial to the luminescence light yield by increasing the particles size and by decreasing the number of quenching defects. Secondly the annealing atmosphere played a major role in the formation of point defects in the material. Annealing in air avoided manganese and oxygen evaporation. The high $Mn^{II}$ content promoted hole trapping at $Mn^{II}_{Mg}$ relative to $Mn^{II}_{Ca}$ and $Mn^{II}_{Mg}$ red emission over $Mn^{II}_{Ca}$ orange one. Although half the content in manganese evaporated on annealing in an Ar–$H_2$ atmosphere, $CaMgSi_2O_6$:Mn luminescence properties were greatly enhanced. XREOL and TSL light yields were improved presumably due to the presence of oxygen vacancies. In TSL an additional peak at 475 K was attributed to electron trapping in oxygen vacancies enhanced LLP at RT.

The paper evidenced that $CaMgSi_2O_6$:Mn materials prepared by sol–gel were very sensitive to the annealing conditions. Typical point defects such as oxygen vacancies were created during this step. The most efficient $CaMgSi_2O_6$:Mn material in terms of long-lasting phosphorescence was obtained on annealing in Ar–$H_2$ at 1100 °C, which, if intensified, ultimately provoked the degradation of the structure and the total evaporation of manganese. Therefore annealing in Ar–$H_2$ should be carried out by preserving a trade-off between the $Mn^{II}$ content and the formation of favourable oxygen vacancies.

## Acknowledgements

This work was financially supported by French ANR project Natlurim. The authors acknowledge travel support from Department of Science and Technology, Government of India under Indo-Italian P.O.C for proposals 20090053 and 20100055. Luca Olivi and Giulana Aquilanti from Elettra, Trieste are gratefully thanked for experimental support. The authors are grateful to the Indo-French Centre for the Promotion of Advanced Research (IFCFAR)/CEntre Franco-Indien Pour la Recherche Avancée (CEFIPRA) for support.

## References

1 E. Newton Harvey, *A History of Luminescence: From the Earliest Times until 1900*, Amer. Phil. Soc., Philadelphia, 1957.
2 T. Matsuzawa, Y. Aoki, N. Takeuchi and Y. J. Murayama, *J. Electrochem. Soc.*, 1996, **143**, 2670.
3 A. J. J. Bos, P. Dorenbos, A. Bessière and B. Viana, *Radiat. Meas.*, 2008, **43**, 222.
4 A. Lecointre, A. Bessière, A. J. J. Bos, P. Dorenbos, B. Viana and S. Jacquart, *J. Phys. Chem. C*, 2011, **115**, 4217.
5 A. J. J. Bos, P. Dorenbos, A. Bessière, A. Lecointre, M. Bedu, M. Bettinelli and F. Piccinelli, *Radiat. Meas.*, 2011, **46**, 1410.
6 T. Aitasalo, *J. Solid State Chem.*, 2003, **171**, 114.
7 Q. le Masne de Chermont, C. Chanéac, J. Seguin, F. Pellé, S. Maîtrejean, J.-P. Jolivet, D. Gourier, M. Bessodes and D. Scherman, *Proc. Natl. Acad. Sci. U. S. A.*, 2007, **104**, 9266.
8 T. Maldiney, A. Lecointre, B. Viana, A. Bessière, M. Bessodes, D. Gourier, C. Richard and D. Scherman, *J. Am. Chem. Soc.*, 2011, **133**, 11810.
9 A. Lecointre, A. Bessière, B. Viana and D. Gourier, *Radiat. Meas.*, 2010, **45**, 497.

10 L. Jiang, *J. Alloys Compd.*, 2004, **377**, 211.
11 Y. Chen, X. Cheng, M. Liu, Z. Qi and C. Shi, *J. Lumin.*, 2009, **129**, 531.
12 A. Lecointre, A. Bessière, K. R. Priolkar, D. Gourier, G. Wallez and B. Viana, Role of $Mn^{II}$ doping in red long-lasting phosphorescence of $CaMgSi_2O_6:Mn^{II}$ diopside for *in vivo* imaging, *Mater. Chem. Phys.*, submitted.
13 M. Newville, *J. Synchrotron Radiat.*, 2001, **8**, 322.
14 B. Ravel and M. Newville, *J. Synchrotron Radiat.*, 2005, **12**, 537.
15 B. Ravel, *J. Synchrotron Radiat.*, 2001, **8**, 314.
16 S. I. Zabinsky, J. J. Rehr, A. Ankudinov, R. C. Albers and M. J. Eller, *Phys. Rev. B: Condens. Matter*, 1995, **52**, 2995.
17 A. L. Ankudinov, A. I. Nesvizhskii and J. J. Rehr, *Phys. Rev. B: Condens. Matter*, 2003, **67**, 115120.
18 L. Levien and C. T. Prewitt, *Am. Mineral.*, 1981, **66**, 315.
19 J. R. Harbridge, G. A. Rinard, R. W. Quine, S. S. Eaton and G. R. Eaton, *J. Magn. Reson.*, 2002, **156**, 41.
20 J. A. Weil, *Phys. Chem. Miner.*, 1984, **10**, 149.

 